Development of a design tool for closed-loop digital vibrometer

Dario Melchionni, Alessandro Magnani, Alessandro Pesatori, and Michele Norgia*

DEIB, Politecnico di Milano, Milano 20133, Italy

**Corresponding author: michele.norgia@polimi.it*

Received 6 August 2015; revised 15 October 2015; accepted 15 October 2015; posted 16 October 2015

1. INTRODUCTION

Classic interferometry is based on two coherent beams, generated by the same laser and combined by two different length optical paths, one of reference and one of measurement, to produce a phase-dependent signal used typically to reconstruct velocity or displacement. Different from the classical one, self-mixing interferometry needs only one optical path to generate the interferometric signal [1–3] to be read. This interferometric technique uses the laser cavity itself as a receiver and path of reference; the light beam scattered by the target is partially collected and injected again in the cavity where it interferes with the lasing beam. The result is an electromagnetic signal that is related with the laser power reinjected and so with movement of the target. At this point, it is possible to read this signal by monitoring the optical power everywhere along the path and retrieve information about the target or directly inside the laser cavity through the monitor photodiode placed on the chip [1].

This configuration is naturally self-aligning and it has a huge potential for user-friendly and low-cost applications. However, amplitude, shape and time-variant characteristics of the interferometric signal are the function of many variables [4], so increasing the system complexity and the capability of reading correctly the measurement. A deep system analysis is required especially when the self-mixing technique is carried out by performing a closed-loop laser control aiming to go further than the sensitivity limit reached by the open-loop configuration [5].

The aim of this work is the development of modeling tools able to describe a self-mixing vibrometer working in closed-loop configuration and then to design and validate a custom control which guarantees the best performance in term of bandwidth, noise-equivalent displacement (NED), and stability.

2. CLOSED-LOOP TECHNIQUE

The closed-loop technique has born to overcome the resolution limit, which is intrinsically bounded to the fringes counting elaboration performed in open-loop configuration [5,6].

In Fig. 1, an example of signals obtained from a target sinusoidal vibration monitored by an open-loop vibrometer exhibits the typical interferometric shape, which depends on the feedback coefficient C [3,4]. According to the theory, the signal is distorted, while each fringe matches with a target movement equal to $\lambda/2$, where λ is the LD wavelength. The information about displacement is retrieved by means of counting the fringes number even if with a limited resolution of $\lambda/2$.

The measurement is quite robust and guarantees the same resolution regardless of the C factor [7–11] of the interferometric signal. The closed-loop has been proposed for broadening the sensitivity by evaluating the signal inside a single fringe. In that way, the measurement error due to the distortion is negligible, and the measurement is limited only by noise [6]. In order to understand the operating principle, it is useful to consider Fig. 2, where few fringes are depicted: β, the slope of the fringe in [W/rad], is supposed to be linear. The more back-injection increases, the more this assumption is justified; in fact, as is shown in Fig. 1, for middle-high back-injection ($C \geq 1$) the interferometric signal gets closer to a sawtooth wave.

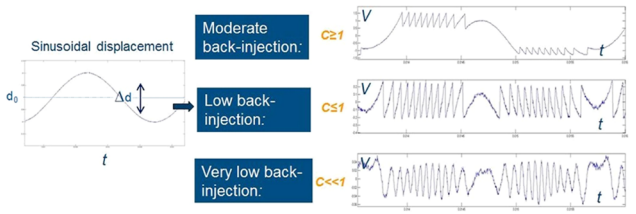

Fig. 1. Signal obtained over a target with sinusoidal displacement for different C values.

According to classical self-mixing optical setup [1], the optical phase shift between emitted and back-injected light is equal to:

$$\varphi_{\text{opt}} = 2 \cdot \left(\frac{2\pi}{\lambda}\right) d_0, \tag{1}$$

where λ is the wavelength of the light and d_0 the absolute distance between laser and target. The φ_{opt} term is a function of both the distance and the laser wavelength; by differentiating Eq. (1), it is possible to express the phase variation as follows:

$$\delta\varphi_{\text{opt}} = \left(\frac{4\pi}{\lambda}\right)\delta d_0 - \left(\frac{4\pi d_0}{\lambda^2}\right)\delta\lambda = L_s \cdot \delta d_0 - L_\lambda \cdot \delta\lambda. \tag{2}$$

If we consider small variations around a middle fringe working point under middle-high back-injection condition, Eq. (2) states that both target movement and a wavelength shift cause interferometric signal variations, due to the direct linear relationship:

$$\Delta P_{\text{S.M.}} = \beta\Delta\varphi. \tag{3}$$

A feedback system sets the working point, by modulating the LD wavelength to compensate for the distance variation. According to the control system theory, the loop erases the phase variations as much as the loop gain is high. Ideally, the feedback keeps constant the number of wavelengths along the optical path:

$$\delta\varphi_{\text{opt}} = 0 \rightarrow \Delta\lambda = \left(\frac{\lambda}{d_0}\right)\Delta d_0. \tag{4}$$

Actually, the real loop has finite bandwidth and gain; as a result, target movement is not perfectly compensated by the wavelength modulation. The working point drifts following d_0 until it reaches the fringe boundaries, and a fringe jump occurs. However, thanks to the loop effect, the error signal assumes the classical self-mixing waveform enlarged by a factor proportional to the loop gain:

$$\Delta d_{\text{closed-loop-fringe}} = \left(\frac{\lambda}{2}\right) \cdot G_{\text{loop}}. \tag{5}$$

In other words, the linear interval of the transfer function is G_{loop} times wider than the open-loop one; β distortions are attenuated by a factor equal to G_{loop} according to Bode's Theory. Thus, assuming the nonlinearity negligible, the sensitivity is limited only by the noise when d_0 variation is less than $\Delta d_{\text{closed-loop-fringe}}$.

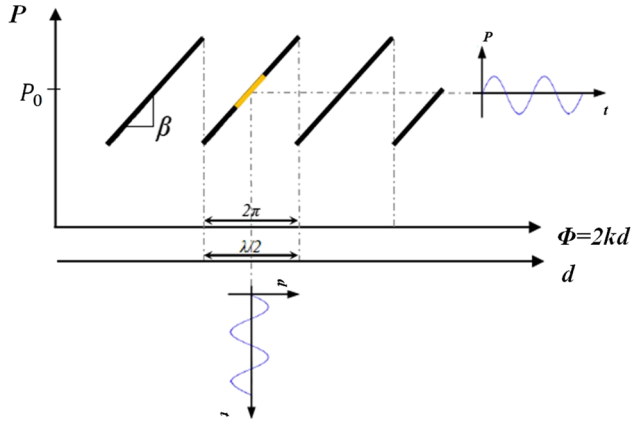

Fig. 2. A generic variation of the optical phase causes the linear modulation of the interferometric signal, whether $C \geq 1$.

3. BLOCK DIAGRAM

This paragraph describes in detail the system block diagram, the starting point to accomplish the simulation. The block combines the ideal scenario, summarized in Section 2, and the peculiarities identified by testing the realized prototypes. The results explanation starts from a simple core, and then grows in complexity by following the same cognitive process adopted during the research.

The LD wavelength is modulated in order to compensate the effect of target vibration. The feedback guarantees the balance by modifying the laser current in the function of the interferometric signal read from the monitor photodiode. Figure 3 shows the block diagram; in block A, ΔV represents the voltage output due to the phase variation $\Delta\varphi$; ΔP, optical power variation, is obtain as explained by Eq. (3) and converted into current I_{ph} by the photodiode with responsivity σ [A/W]. Finally, the current is amplified by a transimpedance stage, Z. The resulting transfer function is:

$$\Delta V = \beta\sigma Z\left(\frac{4\pi}{\lambda}\right)\Delta d_0. \tag{6}$$

In addition, the sub-blocks describe the phase contributions $\Delta\varphi\backslash\Delta\lambda$ and $\Delta\varphi\backslash\Delta d$ explained above. In particular, $\Delta\varphi\backslash\Delta\lambda$, is controlled by the feedback through the laser current modulation.

The branch designed in block B closes the loop by injecting the transimpedence output ΔV into the laser diode through the admittance $Y = 1/Zin$. The loop sets the operating point by establishing the DC laser current which is regulated by ΔV_0. The comparison between ΔV_0 and ΔV returns the error signal that, after the elaboration of the regulator $R(s)$ (described in the next paragraphs), is used to modulate the LD current. It is interesting to notice that the operating point is fixed when d_0 and ΔV_0 are determined. Uncertainty of target position results in uncertainty of operating point, which is potentially dangerous for stability. In the worst case, when the loop works where the interferometric signal shows a positive β, the loop gain is no longer negative; thus, the system is unstable. At least, if the point where the system is supposed to work drifts away from

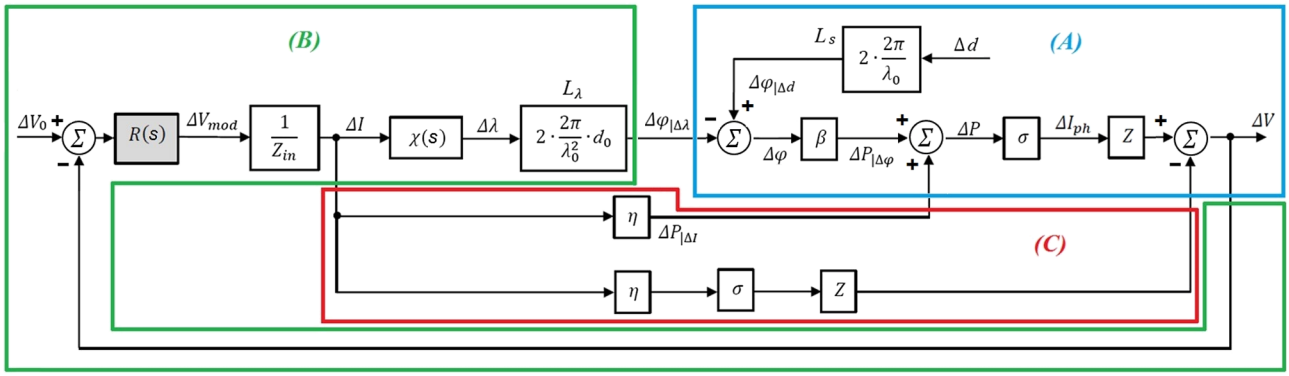

Fig. 3. Closed loop vibrometer block diagram.

the half-fringe, the dynamic is reduced, and a fringe jump occurs for a target movement smaller than $\Delta d_{\text{closed-loop-fringe}}$.

Another nonideality concerning the dynamic is given by the limited laser current range. Clearly, when the laser polarization current reaches its maximum value, 130 mA (or the threshold, about 50 mA), it is not possible to increase the modulation.

The loop gain equation deduced from the blocks A and B system is:

$$L(s) = -\frac{Z\beta\sigma\chi(s)R(s)}{Z_{in}}\left(\frac{4\pi d_0}{\lambda^2}\right), \tag{7}$$

where $\chi(s) = \partial\lambda/\partial I$ is the wavelength modulation coefficient and describes how the temperature variation due to current modulation affects the laser cavity dimensions and, as a consequence, the LD wavelength.

Also, the evaluation of the instrument sensitivity, S, is very important:

$$S = \frac{\Delta V}{\Delta d_0} \cong \left(\frac{\lambda Z_{in}}{R(s)\chi(s)d_0}\right). \tag{8}$$

The characterization allows understanding which singularities are introduced and if these significantly affect the system. In the literature, this topic has been discussed [12]; however, the laser characterization is always required to identify its specific role in the custom system design. For this work, $\chi(s)$ has been obtained and taken into account in the simulation, even if details have been omitted.

We have to take into account another effect of laser behavior; a direct power modulation occurs when the bias current is modulated. The output light power variation $\Delta P|_{\Delta I}$ is detected by the photodiode, and this second signal is superimposed to $\Delta P|_{\Delta\varphi}$ concurring to create ΔP. Compensation, summed up in block C, Fig. 3, has been designed to erase this contribution due to the laser diode slope efficiency η [W/A]. The second branch, dedicated to cancel the power modulation and defined by Eq. (9), avoids two problems: first, the transimpedance stage saturation and, second, the system instability.

$$\text{Compensation\_gain} = -\frac{Z\sigma\eta}{Z_{in}}. \tag{9}$$

Under the hypothesis of low error subtraction, the vibrometer sensitivity remains equal to Eq. (8) and all the parameters are known except the target distance d_0, which can vary from one measurement to another. However, an instrument calibration can easily solve the problem by monitoring the target distance. Well-known interferometric technique for absolute distance measurement [13,14] can be applied with the same laser source.

The block diagram in Fig. 3 is the first step to build a reliable simulation tool, suitable for designing and testing the digital regulator $R(s)$. The next paragraph describes the *Matlab/Simulink* models of the analog and digital signals.

4. OPEN LOOP SIMULATION WITH M PARAMETER CORRECTION

A model for describing the nonlinear phenomena involved in self-mixing interferometry has been the starting point for closed loop study development [5]. It is based on schematic block diagrams and allows using of powerful and standard simulation tools such as *Spice*, *VHDL-AMS* or *MATLAB/Simulink*. In order to study the closed-loop system, a very precise model was developed in *MATLAB/Simulink*, for describing the interferometric signal as function of target vibration, back-injection factor C and α [15]. The open-loop vibrometer is completely described by combining the model and the block diagram in Fig. 3.

Figure 4 shows a comparison between the simulated signal and a real measurement. The experimental signal has been measured through the built-in package photodiode when the target at distance $d_0 = 82$ cm vibrates at 150 Hz with a vibration amplitude of 3.5 μm The same data have been used for the

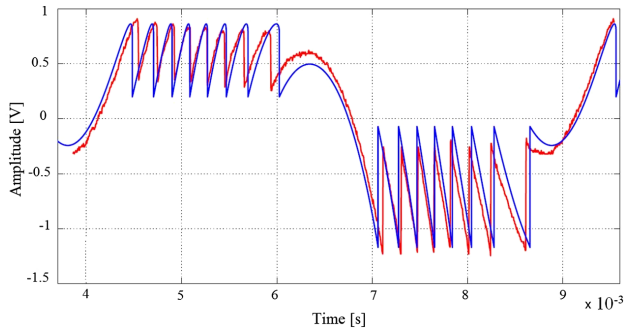

Fig. 4. Comparison of simulation output (blue line) and acquired fringes (red line). The simulation matches the experimental signal.

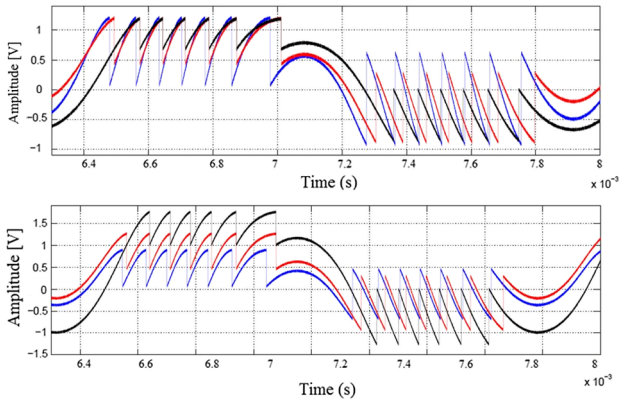

Fig. 5. Signal generated with the enhanced model: the signal increases when C factor rises according to the real interferometric signal behavior.

simulation; in addition we considered $\alpha = 4.5$ and $C = 6$. The signals show a good agreement; in particular, the model calculates amplitude and shape variations taking into account the amount of retroinjected power. Small phase differences are derived from errors of fractions or fractions of λ in d_0 evaluation. A particular model, already proposed in the literature [16], works by estimating m, percentage of the emitted light power back-reflected into the cavity, always equal to 1×10^{-3}. Experimental acquisitions have shown that the system is sensitive to m variation, and theory states that C can be expressed as follows:

$$C = \frac{m\sqrt{1+\alpha^2}}{\eta_{\text{air}} \cdot L_{\text{cav}}} d_0. \tag{10}$$

Therefore, the coefficient m is given by

$$m = \frac{\eta_{\text{air}} \cdot L_{\text{cav}}}{\sqrt{1+\alpha^2}} d_0 C. \tag{11}$$

Equation (11) is used to express m as a function of C. Figure 5 shows, for three different C values, the self-mixing signal assuming $L_{\text{cav}} = 400$ µm, target distance $d_0 = 80$ cm, $\eta_{\text{air}} = 1$. If we consider the old model, the fringes are shaped due to the C parameter, but the minimum and the maximum values are fixed by m.

5. REGULATOR DESIGN AND ANALOG CLOSED LOOP SIMULATION

In this paragraph, a few examples of regulator $R(s)$ for closed-loop are proposed and tested on a real prototype. As explained before, the instrument performance is determined by the feedback, in particular, stability and bandwidth play a main role by defining the operating range in which the vibration can be successfully hooked and measured. The loop function is expressed as

$$L(s) = G(s) \cdot R(s), \tag{12}$$

where $G(s)$ is the known transfer function between the output transimpedance voltage ΔV and the current modulation voltage ΔV_{mod}. Figure 6 shows $G(s)$, assuming these values for the parameters: $Z = 3.3$ MΩ; $\sigma = 0.010454$ [mA/mW]; $Z_{in} = 119$ Ω; $\beta = 6.610 - 6$ [W/rad]; and $d_0 = 0.82$ m. It follows a low-pass behavior, where magnitude is constant and phase is null until approximately 10 kHz.

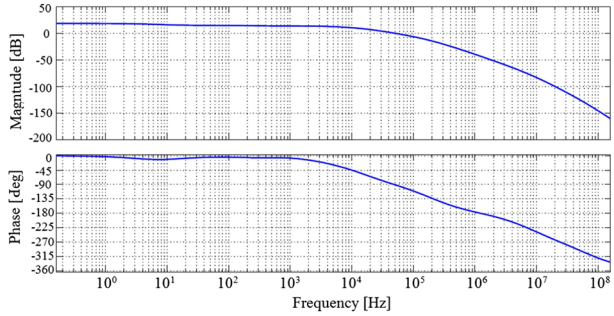

Fig. 6. Comparison of simulation output (blue line) and acquired fringes (red line). The simulation matches the experimental signal.

The loop regulator $R(s)$ performance has been analyzed by using the system control theory sensitivity functions $S(s)$ and $Q(s)$. In this particular system, they can be summarized as shown below:

$$S(s) = \frac{\Delta V(s)}{\Delta d(s)} = L_s \cdot \frac{\sigma\beta Z(s)}{1 + R(s) \cdot Z_{in}(s) \cdot \chi(s) \cdot L_\lambda \cdot \sigma\beta Z(s)}, \tag{13}$$

$$Q(s) = \frac{\Delta I(s)}{\Delta d(s)} = L_s \cdot \frac{\sigma\beta Z(s) \cdot Z_{in}(s) \cdot R(s)}{1 + R(s) \cdot Z_{in}(s) \cdot \chi(s) \cdot L_\lambda \cdot \sigma\beta Z(s)}. \tag{14}$$

Four regulators were designed and compared: proportional controller (R_2), integral controller (R_3), proportional-integral controller (R_4), and a controller built ad-hoc (R_1). The model was identified to approximate the experimental ratio of output to input, rather than derived from a rigorous analytic model. According to this, the singularities might differ from the real ones even if they well describe the measured signals. Under this assumption, particular attention is focused to system robustness, quantified by phase (ϕ_m) and gain margin (k_m). The obtained performance is listed in Table 1 where robustness and bandwidth comparison highlights R_1 and R_4 as preferable solutions.

In detail, the regulators structures are:

$$R_1(s) = \frac{s}{(s + p_{PB})} \cdot \frac{(s + z_{AL})}{(s + p_{PB})}, \tag{15}$$

$$R_4(s) = \mu_4 \cdot \frac{(s + z_{AF})}{s}. \tag{16}$$

Table 1.

Regulator	Phase Margin	Gain Margin	Critical Freq.
$R_i(s)$	ϕ_m – [°]	k_m – [dB]	f_c – [Hz]
$R_1(s)$	51.9	32.1	$9.13 \cdot 10^5$
$R_2(s)$	50	30	$1.76 \cdot 10^5$
$R_3(s)$	49.2	26	$5.31 \cdot 10^5$
$R_4(s)$	52.6	32	$8.86 \cdot 10^5$

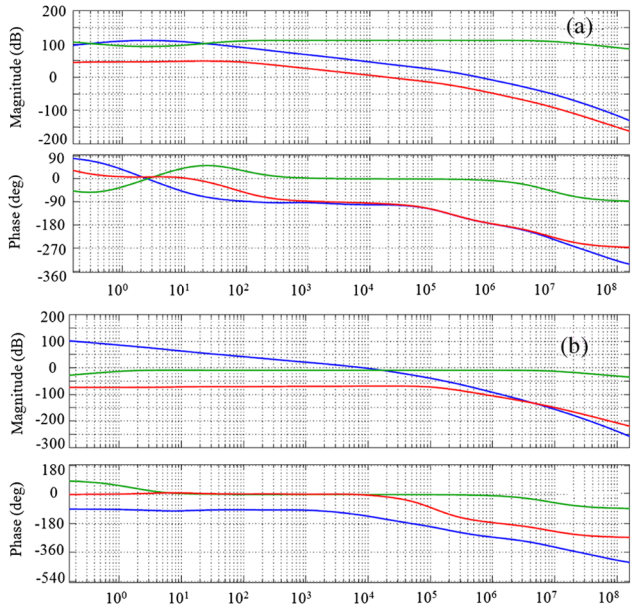

Fig. 7. Regulator: (a) R_1 and (b) R_4: $L(s)$ transfer function (blue), $S(s)$ sensitivity function (green), $Q(s)$ sensitivity control function (red).

Results obtained can be appreciated, also, in Fig. 7 where graphs show the loop transfer and the sensitivity functions as well.

The regulators introduced in the model allow us to simulate, for the first time, the closed-loop configuration. Noise has been added in the simulation in order to better model the real system. The limiting factor in the realized prototype is represented by the photodiode shot-noise, given by Eqs. (17) and (18):

$$I_n^2 = 2qFP_0 \left[\frac{A^2}{\text{Hz}}\right], \tag{17}$$

$$V_{\text{shot}} = \sqrt{I_n^2 \cdot Z^2} = 5.90 \left[\frac{\mu\text{V}}{\sqrt{\text{Hz}}}\right]. \tag{18}$$

The voltage equivalent noise is calculated for power $P_o = 50$ mW, $F = 2$, $\sigma = 0.01$ [A/W], $q = -1.6 \cdot 10^{-19}$ C and $R = 330$ kΩ. Figure 8 shows the *Simulink* block diagram completed with R_1. Closed-loop behavior has been simulated for different scenarios, with frequency sweep and different amplitude variation as well.

As an instance, Fig. 9 shows on the left the open-loop signal, and, on the right, the closed-loop one, with vibration frequency

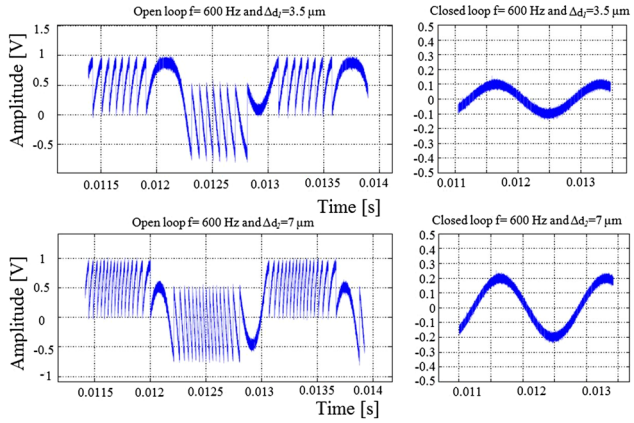

Fig. 9. Simulations comparison between Open-loop and Closed-loop configuration at different vibration amplitude: 3.5 and 7 μm.

equal to $f = 600$ Hz, $C = 4.5$, $\alpha = 3.5$, and vibration amplitudes $\Delta d_1 = 3.5$ μm and $\Delta d_2 = 7$ μm. The simulation demonstrates, at first, that the model is able to describe the closed loop vibrometer behavior and, as a consequence, that it is a powerful instrument for control design.

6. DIGITAL MODEL

Digital feedback development has several advantages; its flexibility allows managing the system complexity, testing different regulators, and processing the signal as required. An additional advantage is offered by a secondary digital output, which potentially allows retrieving the information and, at the same time, to compensate for errors and nonlinearity. At first, when the feedback is not able to suppress all fringes, due to the finite G_{loop}, a jump occurs, and it is directly injected into the laser. Current pulse causes laser instability and, as a consequence, the loop instability. The laser device itself can be affected by sudden current variations too.

An unwrap algorithm [7,10] can be used as a solution; it corrects the fringe jumps digitally and avoids abrupt variation due to nonlinear behavior of the system, when the feedback gain and bandwidth limits are reached. However, the user has to be aware of the fact that a correction occurs, and the measurement reliability decreases. According to this, both a modulation and a nonlinearized digital output need to be implemented. It can be easily done with the help of digital elaboration. Another reason why a second output could be useful is represented by the necessity to overcome the dynamic

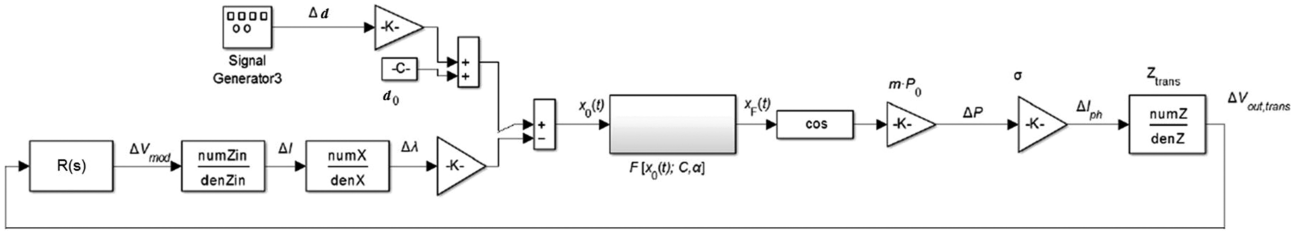

Fig. 8. Closed loop Simulink model.

boundaries. It is possible that the system is driven out of the linearity operating range because the target movement exceeds tracking dynamic, which has been fixed by the maximum modulation current $I_{\text{mod}} \approx 15$ mA. In that case, the loop is not able to catch the vibration again, and the system working point is not well defined. On the other hand, if it is possible to recognize this situation and consequently adapt the laser DC current, the operating point can be shifted as much as possible by the laser source. In that way, $\Delta\lambda$ required to compensate the vibration is achieved mainly by the DC current drift and, in a second time, by the loop controlled modulation.

A digital elaboration can analyze the system working point and broaden the dynamic by executing this shift. The new operating point needs to be registered and the controller modified according to λ and d_0 corrections. The output has to take into account this DC contribution. As before, the measurement is meaningless during the transient, so the instrument output should be blinded. Digital elaboration is also suitable for correcting the instrument sensitivity, which is frequency dependent because of $\chi(s)$. The output voltage is supposed to be a function exclusively of the vibration amplitude, but it is not because of the $(\partial\lambda/\partial I)$ behavior with frequency [12]. A digital signal processing can easily compensate for this contribution and free the output signal from the undesired dependency.

Another potential advantage regards the compensation loop. The laser diode slope efficiency is not exactly known, and it is not linear as well. Experimental acquisitions of transimpedance output signal illustrate that even if the subtraction occurs at low frequency, the signal due to current modulation remains considerable. The main harmonics composition has been retrieved, and a pre-emphasis technique can be adopted to minimize the error, by the means of a look-up table and a dedicated digital output.

For that reason, a digital closed-loop model has been implemented, and it is here described. Instrument prototypes based upon DPS (digital signal processor) have been developed; therefore, it is interesting to consider which differences have been introduced due to signal quantization and discretization.

At first, in the literature, the interferometric signal is sampled with $f_s = 800$ kHz. It is sufficient if we consider the closed-loop bandwidth $\leq$100 kHz. However, the open-loop signal spectrum has high-frequency harmonics, so aliasing occurs as shown in the Fig. 10 simulation.

Therefore, a FPGA (field programable gate array) based prototype has been developed, and $f_s \geq 12.5$ MHz overcomes this problem.

In addition, it has been demonstrated that increasing the elaboration speed brings another positive effect. The digital regulator implementation introduces latency in the loop. It is a function of the elaboration time which has been expressed as a multiple of the sample rate in Eq. (19):

$$H_{\text{delay}}(s) = e^{\left(\frac{N}{f_s}\right)}. \tag{19}$$

In Eq. (20), the loop transfer function revision applied to the FPGA based system takes into account the phase contribution, which is calculated in Eq. (16) with N, the number of clock periods required by the $R_1(s)$ regulator, equal to 5, and $\omega_c = 147.5$ kHz:

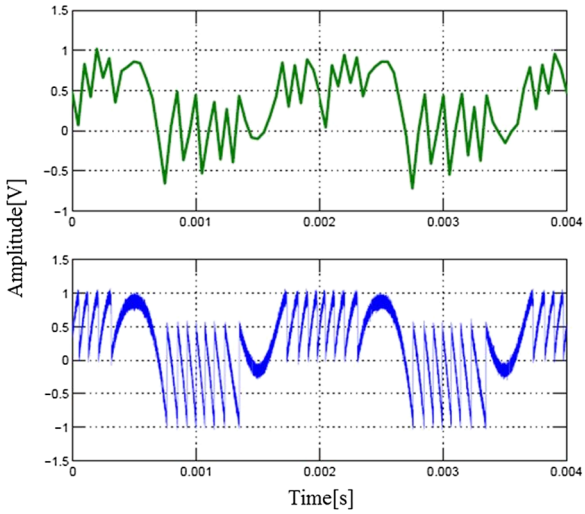

Fig. 10. Aliasing phenomenon occurs in the model with $f_s = 400$ kHz.

$$L_1(s) = G(s) \cdot R_1(s) \cdot H_{\text{delay}}(s), \tag{20}$$

$$\phi_{\text{delay\_FPGA}} = \omega_c \cdot N \cdot \left(\frac{T_{s\text{-FPGA}}}{2}\right) \cdot \frac{180}{\pi} = 10.6°. \tag{21}$$

The phase margin earlier obtained, $\phi_{R_1(s)} = 51°$, is adjusted and loses around 10°; $\phi_{R_1(s)} = 40.4°$, as shown in Fig. 11. It is clear that the stability can be significantly damaged, especially when the elaboration delay increases. According to this, the design solution based on FPGA rather than DSP guarantees better performance.

All these points have been evaluated by means of a digital closed-loop model; a SAR ADC 12 bit model has been introduced to simulate the FPGA data acquisition. $R_1(s)$ has been converted into discrete domain through the Tustin method:

$$R_1(z) = \frac{47z^2 - 94z + 46}{z^2 - 2z + 1}. \tag{22}$$

7. RESULTS

Tests have been conducted to validate the simulation tool comparing the prototype measurement and the model output. One of them is shown in Fig. 12, where the target movement is no

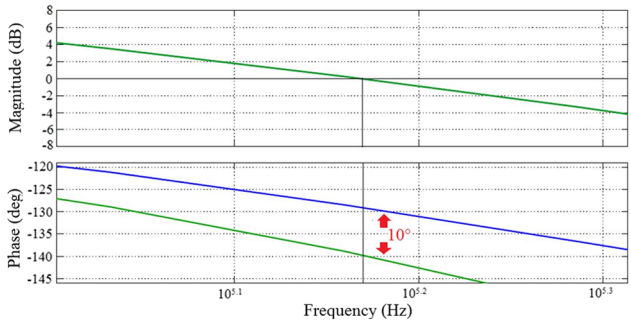

Fig. 11. Phase margin correction derived from elaboration delay evaluation.

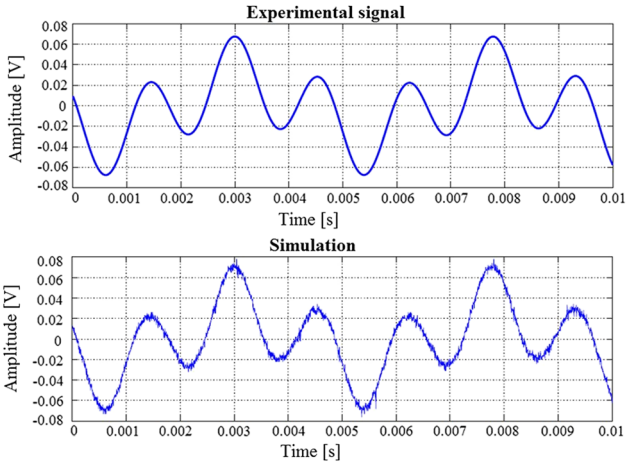

Fig. 12. Comparison between simulation and experimental signal with squared wave input vibration.

more a pure sinusoidal wave; instead, a square wave has been used. In accordance with the physical limits of the loudspeaker used as the target and the closed-loop bandwidth, the two signals show the same harmonics.

The FPGA based prototype shows stability improvement, but almost the same resolution of previous vibrometers. The main issue is the noise and disturbances due to high-frequency digital signal. Thus, NED (noise equivalent displacement) measured is approximately 60 nm, which is comparable with other digital realization. It has been calculated by assuming the instrument noise as the resolution limit and evaluating its root mean square value. However, regulator, high sample frequency, and digital linearization guarantee stability on a 20 kHz bandwidth. The instrument, in particular, shows robustness to C factor variation, in particular when speckle pattern reduces it [17,18]. Vibration tracking also occurs even in the presence of abrupt target displacement validating the control system enhancement. In Figure 12, comparison between the experimental and simulated signal is proposed when the target speaker is driven by a square wave signal. The limited bandwidth allows one to perfectly reconstruct a few harmonics of the original displacement.

8. CONCLUSIONS

Self-mixing closed-loop configuration technique allows us to measure, at a distance of 1 m, with bandwidth between 5 Hz and 20 kHz and a NED of about 60 nm. Stability and dynamic have been improved and can be further enhanced by the means of tools proposed; a simulation model has been built in order to simplify the problem-solving process and the control design. The model developed shows enhancement with respect to previous open-loop versions, and, in particular, describes, for the first time (to the best of the authors' knowledge), the closed loop configuration implemented on a digital device. The simulation toll proposed has been validated by comparing the outputs with the experimental signal acquired. Thus, constraints, weakness, and improvements have been analyzed by double-checking the results obtained both from an FPGA based prototype and computer-based simulation.

Solutions have been created to improve the stability; two kinds of regulator have been proposed and analyzed evaluating the effect of the elaboration delay. Digital technique has been individuated to potentially broaden the instrument dynamic as much as the laser source allows it.

REFERENCES

1. G. Giuliani, M. Norgia, S. Donati, and T. Bosch, "Laser diode self-mixing technique for sensing applications," J. Opt. A **4**, S283–S294 (2002).
2. S. Donati, *Electro-Optical Instrumentation—Sensing and Measuring with Lasers* (Prentice Hall, 2004).
3. R. Lang and K. Kobayashi, "External optical feedback effects on semiconductor injection laser properties," IEEE J. Quantum Electron. **16**, 347–355 (1980).
4. Y. Yu, J. Xi, J. Chicharo, and T. Bosch, "Optical feedback self-mixing interferometry with a large feedback factor c: Behaviour studies," IEEE J. Quantum Electron. **45**, 840–848 (2009).
5. G. Giuliani, S. Bozzi-Pietra, and S. Donati, "Self-mixing laser diode vibrometer," Meas. Sci. Technol. **14**, 24–32 (2003).
6. S. Donati, M. Norgia, and G. Giuliani, "Self-mixing differential vibrometer based on electronic channel subtraction," Appl. Opt. **45**, 7264–7268 (2006).
7. A. Magnani, A. Pesatori, and M. Norgia, "Self-mixing vibrometer with real-time digital signal elaboration," Appl. Opt. **51**, 5318–5325 (2012).
8. U. Zabit, R. Atashkhooei, T. Bosch, S. Royo, F. Bony, and A. D. Rakic, "Adaptive self-mixing vibrometer based on a liquid lens," Opt. Lett. **35**, 1278–1280 (2010).
9. Y. Fan, Y. Yu, J. Xi, and J. F. Chicharo, "Improving the measurement performance for a self-mixing interferometry-based displacement sensing system," Appl. Opt. **50**, 5064–5072 (2011).
10. C. Bes, G. Plantier, and T. Bosch, "Displacement measurements using a self-mixing laser diode under moderate feedback," IEEE Trans. Instrum. Meas. **55**, 1101–1105 (2006).
11. M. Norgia and S. Donati, "A displacement-measuring instrument utilizing self-mixing interferometry," IEEE Trans. Instrum. Meas. **52**, 1765–1770 (2003).
12. M. Norgia, A. Pesatori, M. Tanelli, and M. Lovera, "Frequency compensation for a self-mixing interferometer," IEEE Trans. Instrum. Meas. **59**, 1368–1374 (2010).
13. M. Norgia, A. Magnani, and A. Pesatori, "High resolution self-mixing laser rangefinder," Rev. Sci. Instrum. **83**, 045113 (2012).
14. D. Melchionni and M. Norgia, "Optical system for liquid level measurements," Rev. Sci. Instrum. **85**, 075113 (2014).
15. K. Petermann, *Laser Diode Modulation and Noise* (Kluwer Academic, 1991).
16. C. Bes, G. Plantier, and T. Bosch, "Behavioral model of a self-mixing laser diode sensor," IEEE J. Quantum Electron. **41**, 1157–1167 (2005).
17. J. Ward, D. Kelly, and J. Sheridan, "Three-dimensional speckle size in generalized optical systems with limiting apertures," J. Opt. Soc. Am. A **26**, 1855–1864 (2009).
18. S. Donati, G. Martini, and T. Tambosso, "Speckle Pattern Errors in Self-Mixing Interferometry," IEEE J. Quantum Electron. **49**, 798–806 (2013).